inventions

MDPI

Article

Efficient Protection Scheme Based on Y-Source Circuit Breaker in Bi-Directional Zones for MVDC Micro-Grids

Haider Al-khafaf * and Johnson Asumadu

Department of Electrical and Computer Engineering, College of Engineering and Applied Sciences, Western Michigan University, 1903 West Michigan Ave., Kalamazoo, MI 49008, USA; johnson.asumadu@wmich.edu
* Correspondence: haidermohamed.alkhafaf@wmich.edu

Abstract: A new bi-directional circuit breaker is presented for medium-voltage dc (MVDC) systems. The Y-source impedance network topology is used to implement the breaker. The current transfer function is derived to show the frequency response and the breaker operation with the high frequencies. Mathematical analysis is achieved with different conditions of coupling among the breaker inductors. The minimum level of the magnetic coupling is determined, which is represented by the null condition. The effect of the turns-ratio on this condition is investigated as well. The breaker is designed with two types of fault conductance slope rates. The Y-source breaker is simulated, and the results verify the breaker operation during the fault condition and the load change. The results also demonstrate the effect of the coupling level on the minimum values of the source current when the fault occurs. Based on the expected fault type in the MVDC systems, the proposed breaker is developed to interrupt the overcurrent due to any of these fault types. A protection scheme is proposed for a 12-bus, two-level micro-grid, where the Y-source breakers are used in the bi-directional zones. The results verify the ability of the breaker to conduct and interrupt the current in both directions of the power flow.

Keywords: MVDC grid protection; solid-state DC circuit breakers; coupled inductors; impedance source networks; fault isolation

Citation: Al-khafaf, H.; Asumadu, J. Efficient Protection Scheme Based on Y-Source Circuit Breaker in Bi-Directional Zones for MVDC Micro-Grids. *Inventions* **2021**, *6*, 18. https://doi.org/10.3390/inventions6010018

Academic Editor: Amin Hajizadeh

Received: 9 February 2021
Accepted: 8 March 2021
Published: 10 March 2021

1. Introduction

Due to the developments of the solid-state power transformer (SSPT), medium-voltage dc (MVDC) micro-grids are used to integrate many types of renewable energy sources (RESs), charging stations, electrical vehicles (EVs), and local distribution generators (DGs). The MVDC grids are utilized for that purpose because of their many features such as high efficiency, high controllability, no reactive power, no synchronization problems, no requirements for the output regulation of frequency and voltage, and low cost [1,2]. With these renewable energy sources, the MVDC micro-grids became more desirable. The popular RESs that are integrated into this level of the DC grids are photovoltaics (PVs) and wind farms [3]. Moreover, using MVDC in the distribution systems of modern shipboards is interested in reducing fuel consumption with a larger size of the ship capacity [3,4].

The fault current elimination in the MVDC power systems is considered the main challenge because of the absence of the fault zero-crossing point. In addition, the low impedance characteristics of the MVDC systems causes a high fault current during milliseconds [3,5–10]. For these reasons, the circuit breakers used to interrupt the fault current must have a fast response and create a zero-crossing point naturally during the occurrence of the fault.

The first type of protection device is the molded-case circuit breakers (MCCBs). This breaker contains three main parts, which are a contactor, a quenching chamber, and a thermal-magnetic or electronic tripping device. The tripping device operation depends on the value of the instantaneous current [11]. The MCCBs trip when passing an adequate value of current to heat the thermal-magnetic device and expand the contacts to interrupt

the fault current. The disadvantage of this device is tripping the high-magnitude current during non-faulty conditions, such as the discharging current in the DC grid converter applications [12].

The second type of protection device for the MVDC power systems used semiconductor devices such as insulated gate commutated thyristors, insulated gate bipolar transistors, and gate turn-off thyristors to implement these breakers with a higher capability of the inductive current interruption [13,14]. These types of circuit breakers are hybrid breakers, where a mechanical switch is connected in parallel with the semiconductor device [15–19]. When the fault occurs, the mechanical switch opens, and the fault current is forced to pass through the semiconductor element that interrupts it. Many components are required to add to this breaker, such as metal-oxide varistors (MOVs), capacitors, and switched resistors in order to dissipate the interrupting energy [20,21].

The third type of MVDC circuit breakers is fully solid-state circuit breakers (SSCBs). They have the ability to protect the MVDC grids against the high current during the fault conditions automatically and fast. Many techniques are used to implement the SSCBs, such as using a free-wheeling diode to eliminate the fault current, where the diode is connected across the breaker output. In addition, they can be achieved by using a resonant circuit, where the fault current is dropped to zero naturally [22]. Furthermore, impedance source networks are used to build SSCBs for MVDC systems. The novel sourced-impedance circuit breaker for the MVDC power systems is introduced in [23,24] by using a Z-source impedance network. This network, as mentioned, consists of two inductors and two capacitors that were arranged in the shape of a cross and a Silicon Control Rectifier (SCR). The SCR commutates OFF state due to zero current crossing that is provided by the Z-source network [25–27]. By making these two inductors coupled as in [9], the Z-source breaker can operate with fewer components, smaller size, and reduced weight compared with the non-coupled breaker. The inductor size is reduced by 50% compared with non-couple-inductor Z-source breakers. The coupling of these inductors also provides a path for the reflected current and gives the ability to remove one of the two capacitors that were used in the non-coupled windings breaker [9]. By rearranging these two coupling inductors as in [7], the circuit operates as a coupled-winding Z-source circuit breaker with a Γ shape. Authors in references [7,9] proposed, analyzed, and simulated this circuit with a perfect coupling between these two coils of the breaker. In reference [28], the performance of the Γ shape source impedance breaker was stated under a variable coupling coefficient. The Z-source DC circuit breakers that were produced and designed in the previous work allow the DC current to flow in one direction. The T-source impedance is also presented as a unidirectional solid-state DC circuit breaker in [8]. This topology consists of an SCR, and two coupled inductors with a capacitor were arranged as a T-shape to provide a reverse current forcing the SCR to turn OFF and reduce the source current to zero during the fault conditions.

In many DC power systems, the lines may conduct power in both directions. Therefore, unidirectional circuit breakers are unable to pass the current in the opposite direction. In addition, the capability of the circuit breaker to interrupt the fault current of these lines in both directions of the power flow is required. Based on that, the protection devices that are connected to protect these lines should be bi-directional breakers [29,30].

The purpose of this paper is to propose a new solid-state bi-directional circuit breaker topology for the MVDC systems. The magnetically coupled Y-source impedance network is utilized to implement this breaker. It is developed to operate with two-level MVDC systems. This new work shows the effect of the coupling coefficient and the turns-ratio on the breaker performance during the fault conditions. The breaker is also tested in case the load current changes, and the results show the ability to allow the source to provide the extra load with a higher current without interruption. In this article also, a protection scheme for a 12-bus MVDC micro-grid is implemented. The proposed Y-source impedance circuit breaker is placed in the lines that the bi-direction power flow is expected. The results

proved the ability of the breaker to conduct the current in the opposite direction and to interrupt the source current in case of a fault occurring.

The remainder of the paper is structured as follows: In Section 2, we describe the proposed topology of the Y-source impedance bi-directional circuit breaker; in Section 3, we investigate the proposed topology under fault and load change conditions. We develop the breaker according to the three types of faults that are expected to occur in the MVDC systems. The proposed Y-source breaker also deploys into a 12-bus MVDC micro-grid. Finally, we report the conclusions of the study in Section 4.

2. Proposed Topology (Coupled-Inductor Y-Source Impedance Bi-Directional Circuit Breaker)

A Y-source impedance network is proposed as a bi-directional circuit breaker for MVDC power systems. Three coupled inductors (L_1, L_2, and L_3) and a capacitor are arranged in a Y shape to create the breaker. This topology is able to conduct and interrupt the current in both directions of power flow, as shown in Figure 1. The breaker also contains silicon control rectifiers (SCRs), where these thyristors commutate ON when a triggering gate signal is applied to each thyristor. These signals are removed after the SCRs switch to the ON state; the states of these SCRs are explained in Table 1.

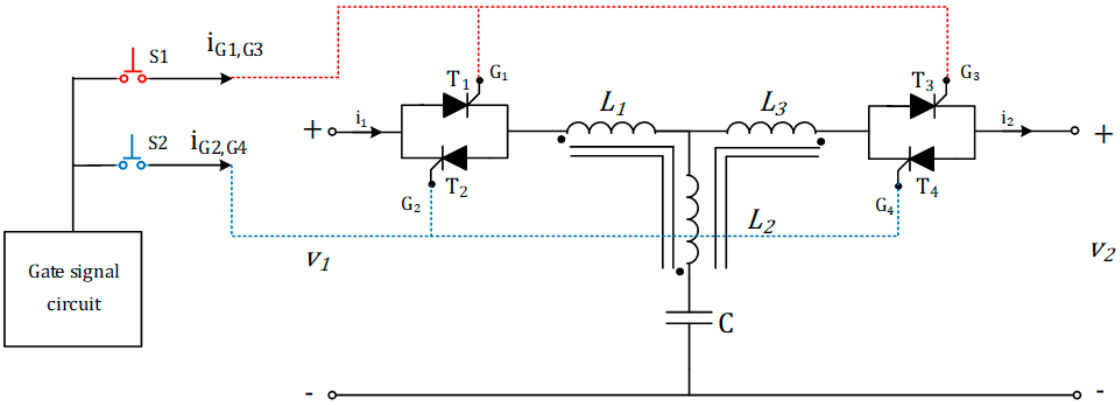

Figure 1. The proposed bi-directional Y-source coupled inductors DC circuit breaker.

Table 1. Gate signals of the Silicon Control Rectifiers (SCRs).

SCR Gates	i_1 and i_2 Direction	
	Positive	Negative
G_1	1	0
G_2	0	1
G_3	1	0
G_4	0	1

The states of the gate signals are 1s when a positive DC voltage from the gate signal circuit is applied from the triggering circuit, as shown in Figure 1. The push-button, S1, is used to send the gate signals to G_1 and G_3 of the SCRs T_1 and T_3, respectively, to turn them ON at the same time. The power direction, in this case, is from V_1 to V_2. The gate states of the SCRs, T_2 and T_4, are 0s. On the other hand, the push-button, S2 is used to send the gate signals to G_2 and G_4 of the SCRs T_2 and T_4, respectively, to turn them ON at the same time. The power, in this case, flows from V_2 to V_1, and the gate states of the SCRs, T_1 and T_3, are 0s.

2.1. Breaker Operation

Based on the proposed breaker shown in Figure 1, the power flow direction in the normal operation is from V_1 to V_2. The forward steady-state load current passes through

T_1, L_1, L_3, T_3 to the load. However, the load current passes through T_4, L_3, L_1, T_2 to the load in case of the other power direction. During transient current conditions, like fault or load change, the capacitor feeds that current through two inductors, L_2-L_3 or L_2-L_1, depending on the power flow direction. The coupling between the inductors provides a path for the reflected current. In case the opposite current reaches the value of the normal forward current, SCRs will be OFF, which interrupts the source current.

2.2. Circuit Breaker Analysis

Figure 2 explains the equivalent circuit that is used for analyzing the Y-source impedance breaker. The equivalent inductance of the breaker in a matrix form is shown in Equation (1).

$$L_{eq} = \begin{bmatrix} L_{11} & M_{12} & M_{13} \\ M_{21} & L_{22} & M_{23} \\ M_{31} & M_{32} & L_{33} \end{bmatrix} \quad (1)$$

where the diagonal elements, the *Lii*s, for i = 1, 2, 3 are the self-inductances. The off-diagonal elements *Mij*s, are the mutual-inductances between the coils i and j. The mutual inductances, *Mij* can be expressed as shown in Equation (2)

$$M_{ij} = k_{ij}\sqrt{L_{ii}L_{jj}} \quad (2)$$

where $i \neq j$, i = 1, 2, 3, j = 1, 2, 3, and k_{ij} is the magnetic coupling coefficient between ith and jth inductors. Based on the equivalent circuit of the proposed Y-source breaker shown in Figure 2, the mutual inductances M_{12}, M_{13}, and M_{23} are defined by Equations (3)–(5).

$$M_{12} = k_{12}\sqrt{L_{11}L_{22}} \quad (3)$$

$$M_{13} = k_{13}\sqrt{L_{11}L_{33}} \quad (4)$$

$$M_{23} = k_{23}\sqrt{L_{22}L_{33}} \quad (5)$$

where k_{12}, k_{13}, and k_{23} are the coupling coefficients between every two inductors as the numbers present. Since the circuit is symmetrical, $M_{21} = M_{12}$, $M_{31} = M_{13}$, and $M_{32} = M_{23}$.

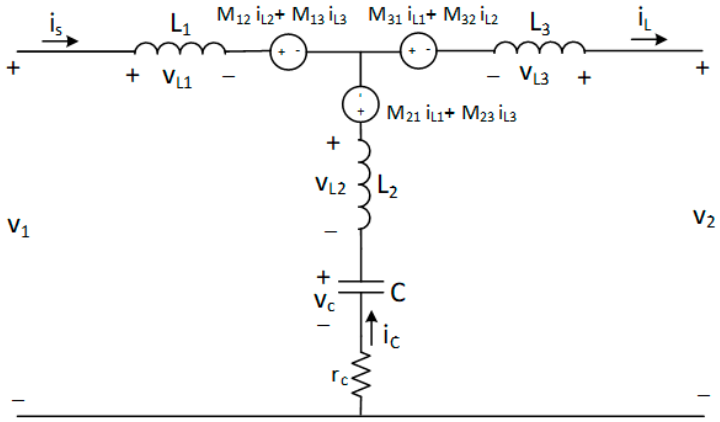

Figure 2. Equivalent circuit of the Y-source breaker.

By substituting Equations (3)–(5) in Equation (1), the matrix form of the equivalent inductance L_{eq} is given in Equation (6)

$$L_{eq} = \begin{bmatrix} L_{11} & k_{12}\sqrt{L_{11}L_{22}} & k_{13}\sqrt{L_{11}L_{33}} \\ k_{21}\sqrt{L_{11}L_{22}} & L_{22} & k_{23}\sqrt{L_{22}L_{33}} \\ k_{31}\sqrt{L_{11}L_{33}} & k_{32}\sqrt{L_{22}L_{33}} & L_{33} \end{bmatrix} \quad (6)$$

The equivalent series resistance (ESR) of the capacitor C is represented by a small resistor r_c as shown in the equivalent circuit of the breaker.

To verify the effect of the coupling coefficient (k) variation on the breaker current gain, the output to the input current transfer function is derived. The equivalent circuit shown in Figure 3 is used to find the current transfer function, where two currents are assumed, as shown in the breaker equivalent circuit.

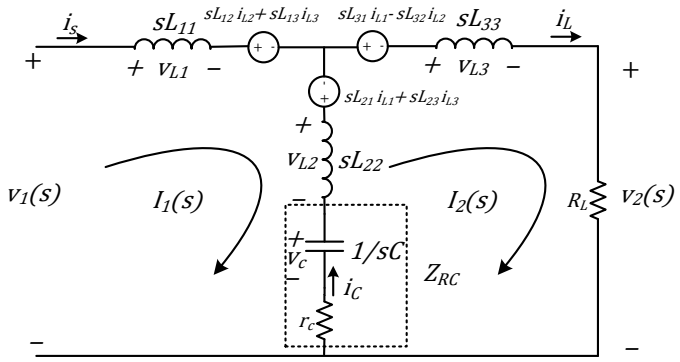

Figure 3. The equivalent circuit of the Y-source impedance breaker.

Two current loops are assumed as shown in Figure 3 to analyze the circuit breaker. Based on these loops, the circuit voltage equations can be written as in Equation (7)

Loop1:

$$v_1(s) = ((L_{11} + 2M_{12} + L_{22})s + Z_{RC})I_1(s) + (-M_{12} + M_{13} + M_{23} - L_{22})s - Z_{RC})I_2(s) \quad (7)$$

Loop2:

$$0 = ((-L_{22} - M_{21} + M_{31} + M_{32})s - Z_{RC})I_1(s) + ((L_{22} - 2M_{23} + L_{33})s + Z_{RC} + R_L))I_2(s) \quad (8)$$

where: Z_{RC} is the equivalent impedance of the breaker capacitor, R_L is the load resistance.

By solving Equations (7) and (8), $I_1(s)$ and $I_2(s)$ are shown below.

$$I_1(s) = \frac{\begin{vmatrix} v_1(s) & (-M_{12} + M_{13} + M_{23} - L_{22})s - Z_{RC} \\ 0 & (L_{22} - 2M_{32} + L_{33})s + Z_{RC} + R_L \end{vmatrix}}{\begin{vmatrix} (L_{11} + M_{12} + M_{21} + L_{22})s + Z_{RC} & (-M_{12} + M_{13} + M_{23} - L_{22})s - Z_{RC} \\ (-L_{22} - M_{21} + M_{31} + L_{32})s - Z_{RC} & (L_{22} - 2M_{32} + L_{33})s + Z_{RC} + R_L \end{vmatrix}} \quad (9)$$

$$I_2(s) = \frac{\begin{vmatrix} (L_{11} + 2M_{12} + L_{22})s + Z_{RC} & v_1(s) \\ (-L_{22} - M_{21} + M_{31} + M_{32})s - Z_{RC} & 0 \end{vmatrix}}{\begin{vmatrix} (L_{11} + 2M_{12} + L_{22})s + Z_{RC} & (-M_{12} + M_{13} + M_{23} - L_{22})s - Z_{RC} \\ (-L_{22} - M_{21} + M_{31} + M_{32})s - Z_{RC} & (L_{22} - 2M_{32} + L_{33})s + Z_{RC} + R_L \end{vmatrix}} \quad (10)$$

From Equations (9) and (10), the current transfer function is given in Equation (11)

$$\frac{I_1(s)}{I_2(s)} = \frac{(L_{22} - 2M_{32} + L_{33})s + Z_{RC} + R_L}{(L_{22} + M_{21} - M_{31} - L_{32})s + Z_{RC}} \quad (11)$$

By substituting Equations (3)–(5) into Equation (11), and the impedance of the breaker capacitor (Z_{RC}) equals r_c + *(1/sC)*, the current transfer function can be written as shown below.

$$\frac{I_1(s)}{I_2(s)} = \frac{s^2C\left(L_{22} + L_{33} - 2k_{23}\sqrt{L_{22}L_{33}}\right) + sC(r_c + R_L) + 1}{C\beta s^2 + sCr_c + 1} \quad (12)$$

where β is defined in Equation (13)

$$\beta = L_{22} + k_{12}\sqrt{L_{11}L_{22}} - k_{13}\sqrt{L_{11}L_{33}} - k_{23}\sqrt{L_{22}L_{33}} \quad (13)$$

In case of perfect coupling between the inductors, the current transfer function becomes as shown below.

$$\frac{I_1(s)}{I_2(s)} = \frac{(L_{22} + L_{33} - 2\sqrt{L_{22}L_{33}})s^2C + sC(r_c + R_L) + 1}{(L_{22} + \sqrt{L_{11}L_{22}} - \sqrt{L_{11}L_{33}} - \sqrt{L_{22}L_{33}})s^2C + sCr_c + 1} \quad (14)$$

The magnitude and phase of the current transfer functions are plotted, as shown in Figure 4. The parameter values of Table 2 are used to plot the breaker current frequency response. In Figure 4a, the values of the coupling coefficient are larger than the null value. In this case, the current response at high frequencies is -5 dB and -2 dB with a coupling coefficient of 90% and 80%, respectively, and the phase is 180°. According to the input-output current frequency response, the breaker produces an opposite output current higher than the SCRs forward current (source current) in case k is more than the null value. This current reduces the forward current less than the holding current and commutates the SCRs to OFF-state.

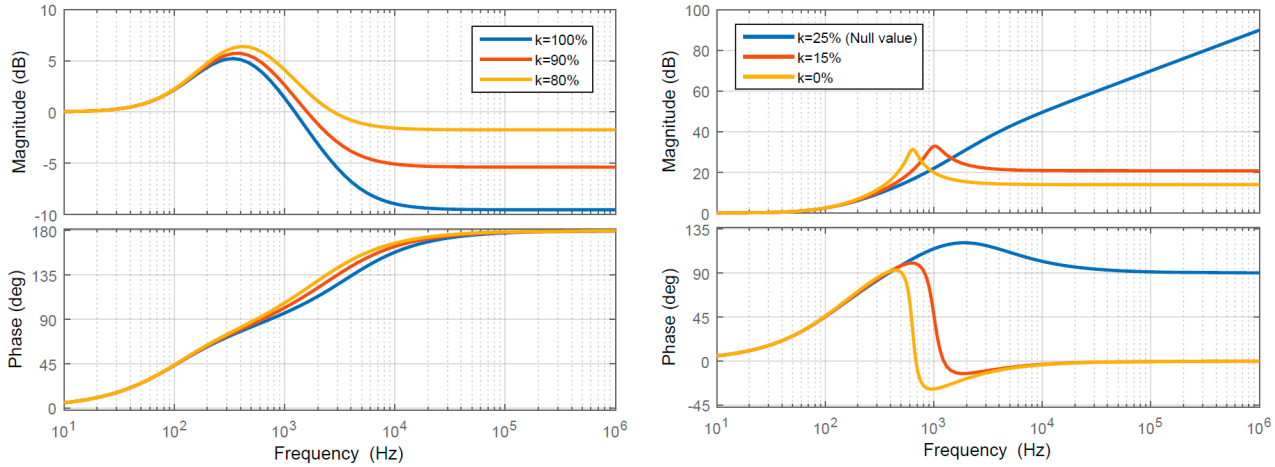

Figure 4. Y-source current frequency response (**a**) k is larger than k_{null} and (**b**) k is smaller than k_{null}.

Table 2. Parameter values of the proposed Y-source circuit breaker.

Parameters	Values	Description
L_1	1000 µH	Self-inductance
L_2	250 µH	Self-inductance [23]
L_3	1000 µH	Self-inductance
C, r_c	100 µF, 0.2 Ω	Capacitance, Equivalent Series Resistance (ESR) [23]
V_1	6 kV	Input voltage [25]
R_L	6 Ω	Load resistance [25]
R_f	10 m Ω	Fault resistance [7]

If case k is equal to the null value, the current high frequencies gain goes to infinity with a constant slope, as shown in Figure 4b. The input current is higher than the output current (positive dB gain). Based on that gain, the current source increases to feed the abnormal current during the fault conditions, and the breaker is unable to interrupt the fault current with k is equal to the null value. The magnitude at high frequencies still has a positive dB gain, and the phase is zero for k less than the null value of the coupling coefficient (k_{null}) as shown in Figure 4b. Two values of the coupling coefficient are chosen to

verify the breaker current response with k less than k_{null}. Based on the frequency response (phase and magnitude), the input current is higher than the output current at the same phase, which keeps the SCRs in the ON-state during the transient conditions.

2.3. Circuit Breaker Design

The fault conductance plays a role in detecting the minimum value of the fault current. This current will be reflected in a different value to break the source current [25]. Some assumptions that are considered in the previous works of [7–9] are used in this work. The load capacitance is also assumed to be zero ($C_l = 0$) [7].

2.3.1. Infinite Fault Conductance Slope Rate

In this analysis, the rising time of the fault conductance is assumed to be zero. The currents of the inductors are also assumed constant. The capacitor of the breaker discharges through the L_2-L_3 to the fault branch when the fault occurs. The discharging current is given in Equation (15)

$$i_c = i_f = G_f V_f \tag{15}$$

where G_f is the fault conductance. The reflected current (i_{ref}) can be expressed as below

$$i_{ref} = k_{12}^2 \cdot \left(\frac{N_2}{N_1}\right)^2 \cdot i_c + k_{13}^2 \cdot \left(\frac{N_3}{N_1}\right)^2 \cdot i_f \tag{16}$$

Assume $k_{12} = k_{13} = k$, the reflected current can be written as below.

$$i_{ref} = \frac{N_2 + N_3}{N_1} \cdot k^2 \cdot i_c \tag{17}$$

To satisfy the condition for breaker operation, the G_f should make the breaker produce a current in the reverse direction to the source with an amplitude that is equal to or greater than the normal steady-state current to force the SCRs to commutate to the OFF-state in order to interrupt the source current. The minimum value of the G_f is shown in Equation (18).

$$G_f \geq \frac{N_1}{N_2 + N_3} \cdot \frac{1}{k^2} \cdot \frac{1}{R_L} \tag{18}$$

Obviously, the G_f is inversely proportional to the square of the coupling coefficient. If case k is decreased to 90%, 82.3% of the load current higher than its normal value makes the breaker reflects enough current to interrupt the source. If case k is unity, increasing 66% in the load current above the normal value is adequate to make the SCRs turn off.

2.3.2. Linear Fault Conductance Slope Rate

In this case, the slope rate of the conductance rises linearly with the time until it reaches its final value, as assumed in [26]. The capacitor current can be written as shown below.

$$i_c = C \frac{dv_f}{dt} \tag{19}$$

where C is the breaker capacitor and v_f is the output voltage when the fault occurs.

From Equations (15) and (19), the fault current can be written as in Equation (20)

$$i_f = G_f V_f = C \frac{dv_f}{dt} \tag{20}$$

where the fault conductance (G_f) equals mt. By solving (20) for v_f, the instantaneous output voltage across the load during the fault ($v_f(t)$) is descripted by the equation below.

$$v_f(t) = v_1 e^{\frac{-m}{2C} t^2} \tag{21}$$

where v_1 is the source voltage. The fault current can be written now as in the Equation below.

$$i_f = v_1 e^{\frac{-m}{2C}t^2} mt \tag{22}$$

At $t = \sqrt{(C/m)}$, the value of the capacitor current is maximum and can be written as below.

$$i_{c(max)} = v_1 \cdot \sqrt{\frac{Cm}{e}} \tag{23}$$

The value of the capacitor current on the N_1 side ($i_c(N_1)$) is shown in Equation (24)

$$i_{c(N_1)} = \left(\frac{N_2 + N_3}{N_1}\right) \cdot v_1 \cdot \sqrt{\frac{Cm}{e}} \tag{24}$$

To satisfy the condition of the reflected current value to commutate the SCR OFF state, Equation (25) describes the minimum value of that slope, which is represented by m_{min}.

$$m_{min} = \frac{1}{k^4} \cdot \left(\frac{N_1}{N_2 + N_3}\right)^2 \cdot \frac{e}{\tau} \cdot \frac{1}{R_L} \tag{25}$$

where τ is the time constant that depends on the R_L and C.

The ability of the breaker to cut off the source current during fault conditions is operative as long as the fault conductance rises with a rate equal to or faster than the rate in Equation (25). From Equation (25), the coupling coefficient k affects the m_{min} with a rate of $(1/k^4)$, where increasing k makes the required value of the slope decrease. By using the values of the parameters as in Table 2, the minimum value of m_{min} is equal to 604 s^{-1} Ω^{-1} with tightly coupled inductors, while with 90% of coupling level, the minimum value of m_{min} is equal to 920.68 s^{-1} Ω^{-1}.

2.3.3. The Effect of Turns-Ratio on k_{null}

The Y-source circuit breaker shown in Figure 1 has three coupled inductors. The first, second, and third inductors have N_1, N_2, and N_3 number of turns, respectively. The numbers of turns for the coupled inductors have a direct effect on the minimum value (null value) of the coupling coefficient. At this value, the term of $C\beta s^2$ in the Equation (12) disappears. At this condition, the k_{null} is shown below.

$$k_{null} = \frac{L_{22}}{\left(\sqrt{L_{11}L_{33}} + \sqrt{L_{22}L_{33}} - \sqrt{L_{11}L_{22}}\right)} \tag{26}$$

The inductance of a coil $L = (1/C_{core}).N^2$, where N is the number of turns and C_{core} is the constant of magnetic core physical characteristics [31]. The magnetic coupling between the inductors can be expressed as shown in Equation (27) with the same magnetic core characteristics.

$$k_{null} = \frac{N_2^2}{N_1N_3 + N_2N_3 - N_1N_2} \tag{27}$$

When the value of k is equal to or less than the value in Equation (27), the breaker cannot interrupt the abnormal current. Figure 5 illustrates the effect of the turns ratio on the null value of k. This value of k becomes higher when the turns-ratio increases. For Figure 5, in case the coils have an equal number of turns, the breaker cannot work even though the coils are tightly coupled. In that aspect, increasing the value of the turns ratio gives the Y-source circuit breaker a wide range of coupling levels to work with.

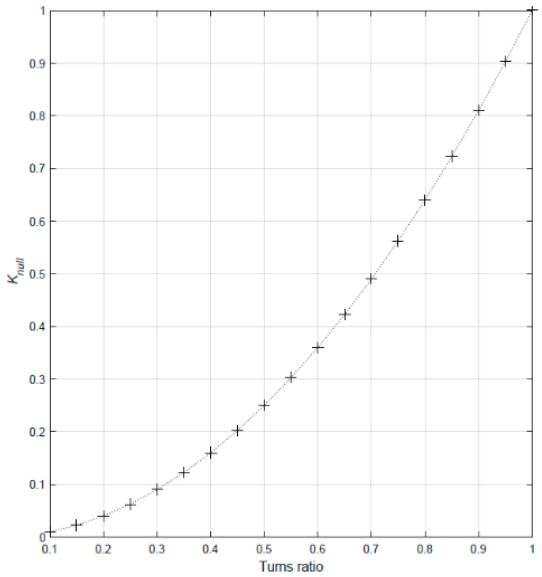

Figure 5. k_{null} with different values of the turns-ratio.

3. Results and Discussions

3.1. Coupled-Inductor Y-Source Impedance Bi-Directional Circuit Breaker

In this section, the proposed topology, illustrated in Section 2, is investigated under fault condition and load change. The investigation has been accomplished using a 6 kV DC source to supply the load through the proposed breaker.

3.1.1. Fault Interruption

In order to verify the operation of the Y-source impedance DC circuit breaker with different values of the coupling coefficient *k*, three coils magnetically coupled have been simulated with a 6Ω load resistance. A 10 mΩ is applied across the load resistance after 200 ms, where this resistance represents a fault resistance. The rest of the parameters are in Table 2. The source-current response in the time domain with different values of the coupling coefficient is shown in Figure 6. These three values of the coefficient are above the null value. In Figure 6a, where the turns-ratio equals 2, the first value is chosen to reduce the source-current to zero. The two other values of the coefficient are randomly chosen to show different minimum values of the source-current ($i_{source(min)}$) during the occurrence of the fault. This simulation was also repeated with another value of L_2, as in Figure 6b. Table 3 shows the minimum values of the source current at the moment of the fault occurring for different values of the coupling coefficient.

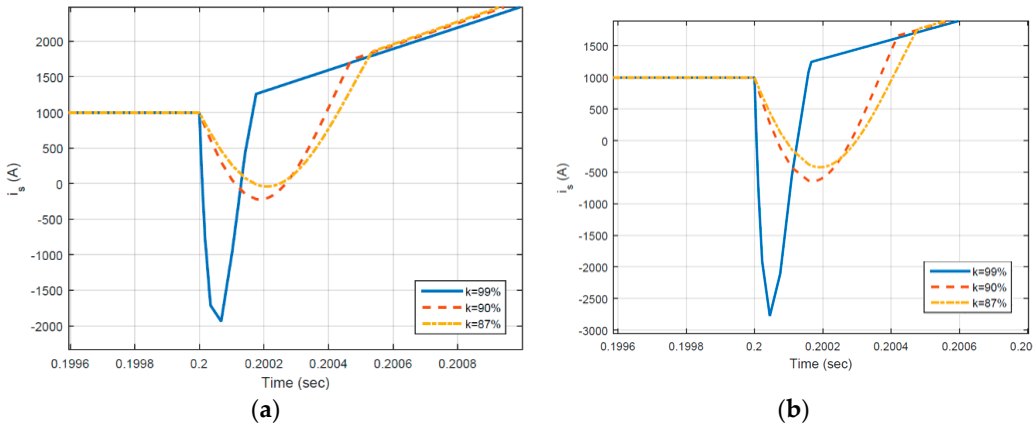

Figure 6. Source current during fault occurring for three different values of *k*. (**a**) Turns-ratio = 2 and (**b**) Turns-ratio = $\sqrt{8}$.

Table 3. Minimum values of the source current with deferent values of the turns-ratio and *k*.

Coupling Coefficient (*k*)	Source Current (A)	
	$N_1/N_2 = 2$	$N_1/N_2 = \sqrt{8}$
99%	−1937.384	−2777
90%	−223	−643
87%	−40.25	−422.5

3.1.2. Load Change

In the second case of simulation, the load current is increased by 50% of its normal value. The source current in this condition decreases and then increases to feed the new load without interrupting the power. The capacitor current increases due to the transient situation and then drops to zero again. Figure 7 shows the source and capacitor current waveforms during the load current change.

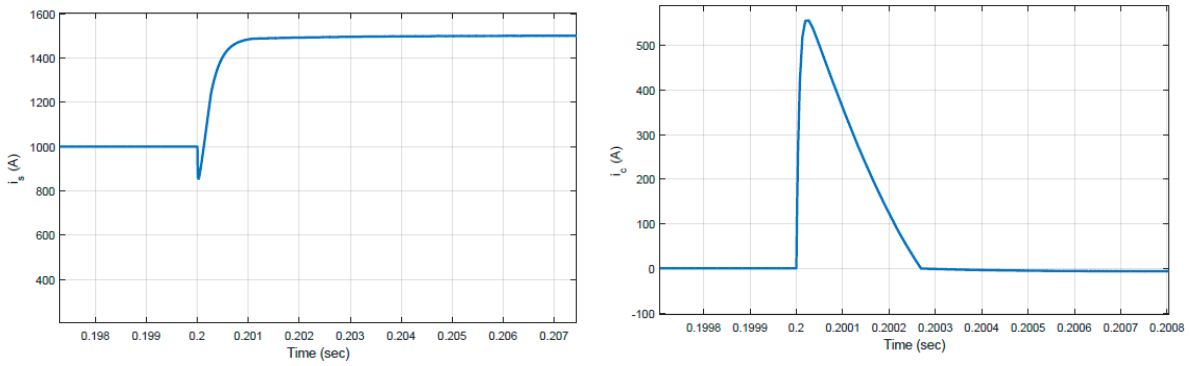

(**a**) (**b**)

Figure 7. Load change simulation results. (**a**) Source current and (**b**) capacitor current.

3.2. Developed Y-Source Bi-Directional Circuit Breaker

In the DC power system configuration, there are three different basic types of fault that are expected to occur. The fault type expectation depends on the system voltage level. These types of faults include a pole-to-pole short circuit (P-P), positive pole-to-Ground Fault (P-G), and negative pole-to-ground fault (N-G) [32]. The circuit breaker of the Y-source topology that is illustrated in Figure 1 is connected through the positive pole of the system. This topology works as a bidirectional breaker in case a fault occurs between the positive pole and the second pole, where it could be a ground or negative pole.

According to the aforementioned faults that are expected to occur in the MVDC systems, the breaker topology has been developed as shown in Figure 8. The parameter values are the same as in Table 2, and v_s is equal to ±6 kV. This topology is able to operate with a two-level DC system where the negative pole is also connected to the load through a Y-source impedance network. The capacitor across the output port is used to force the other pole SCRs to be OFF and interrupts the current that is fed by that pole.

3.2.1. Positive Pole-to-Ground Fault

In case a fault occurs at point F_1, shown in Figure 8, to the ground, the Y-source impedance that is connected to protect the positive pole will interrupt the current supplied by that pole. The fault current will only be supplied by the negative pole (i_{fn}) in case there is no terminal capacitor (C_t). Equation (28) describes the value of i_{fn}.

$$i_{fn} = \frac{\frac{v_s}{2}}{R_f} \tag{28}$$

The terminal capacitor (C_t) that is connected to the breaker terminal is to discharge through the fault path during the moment the short circuit occurs. The transient current of this capacitor activates the operation of the negative pole Y-source network. The reflected current in the primary negative pole inductor (L_{n1}) causes the SCRs to commutate to the OFF state and interrupt the negative source current. Figure 9 shows the simulation results of the current waveforms of the positive pole, negative pole, and terminal capacitor.

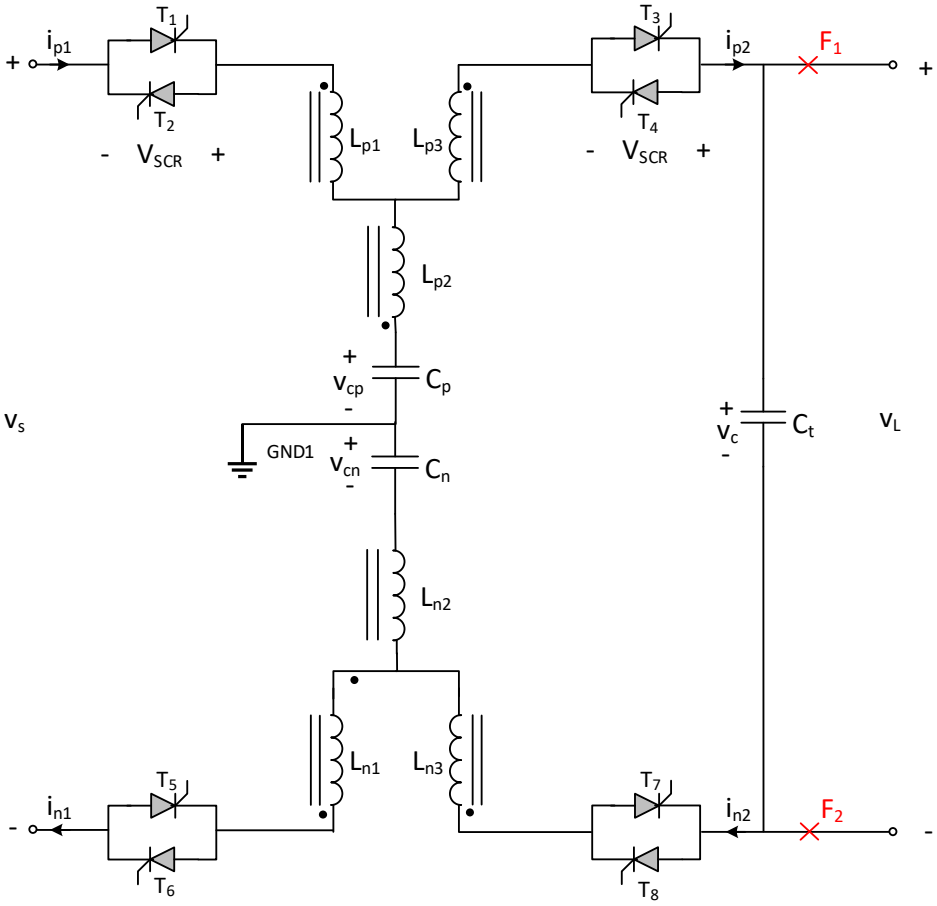

Figure 8. Two levels bi-directional Y-source circuit breaker.

3.2.2. Negative Pole-to-Ground Fault

In this case, the negative pole is shorted to the ground at point F_2, as illustrated in Figure 8. The negative Y-source impedance will control the fault current and reduce it to zero. The fault current that is supplied by the positive pole (i_{fp}) will be limited to the value as in the Equation below:

$$i_{fp} = \frac{\frac{v_s}{2}}{R_f} \tag{29}$$

The terminal capacitor (C_t) acts the same as in the previous case, where it discharges through the fault path when the short circuit occurs. The transient current activates the operation of the positive Y-source network to force the current of that pole to go to zero due to the reflected current in the primary positive pole inductor L_{p1}. Figure 10 shows the current waveforms of the positive pole, negative pole, and terminal capacitor.

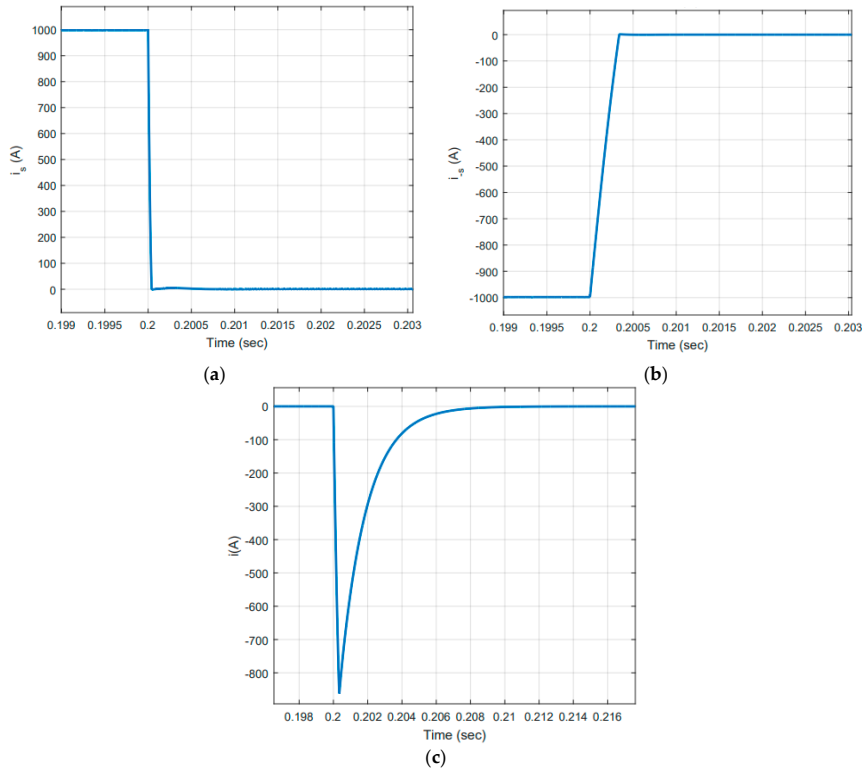

Figure 9. Positive pole-to-ground fault. (**a**) Positive pole current, (**b**) negative pole current, and (**c**) terminal capacitor current.

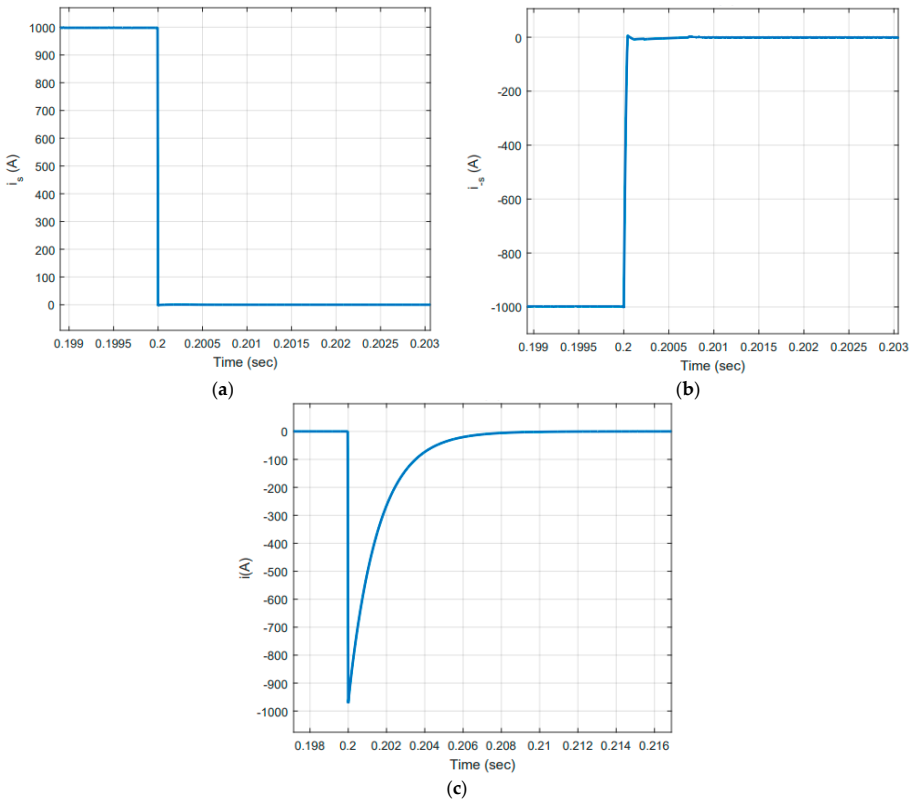

Figure 10. Negative pole-to-ground fault, (**a**) positive pole current, (**b**) negative pole current, and (**c**) terminal capacitor current.

3.2.3. Pole-to-Pole Fault

If case s fault occurs between the points F1 and F2, shown in Figure 8, the rising in the current due to the fault occurring causes a reflected current in the primary inductor of the Y-source impedance in both poles (positive and negative), where the voltage of each pole is 6 kV. The reflected current decreases the SCRs current to zero in both poles, as shown in Figure 11a,b. The terminal capacitor discharges through the fault path, as shown in Figure 11c. Compared to the two previous types of faults, the value of the capacitor discharging current is higher when a pole-to-pole fault occurs.

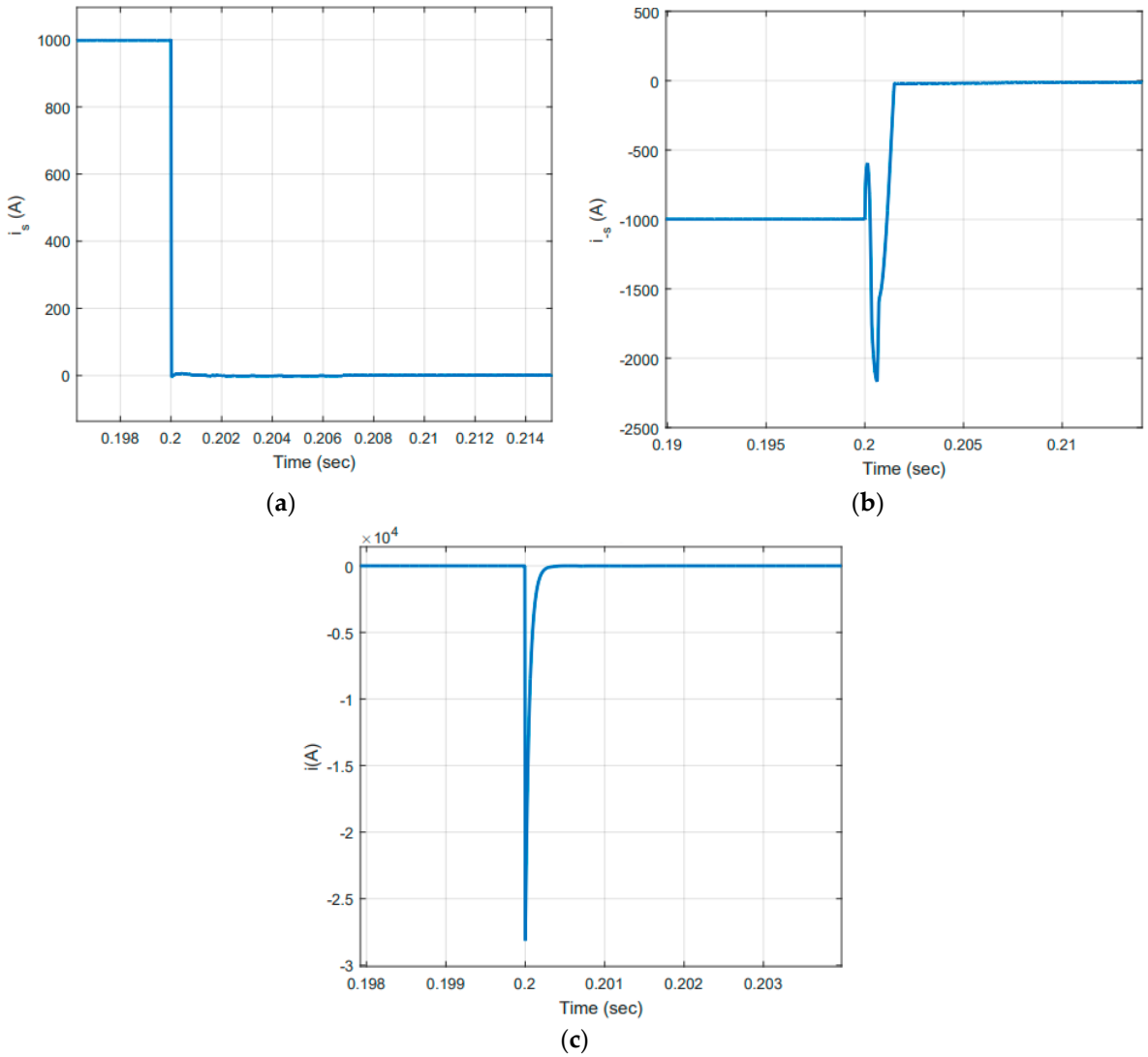

Figure 11. Pole-to-pole fault, (**a**) positive pole current, (**b**) negative pole current, and (**c**) terminal capacitor current.

3.3. Y-Source Breaker Deployment into MVDC Micro-Grid (Case Study)

A 12-bus MVDC micro-grid is presented for the proposed protection scheme, as shown in Figure 12. The microgrid is structurally similar to the test MVDC micro-grid in [32,33]. The voltage level of this grid is ±2.5 kV, which is the typical voltage for medium voltage DC systems [34]. The utility grid is connected through a two-level voltage source converter (VSC) at bus1, where this VSC controls the DC voltage of the MG. A local AC generator (DG) is connected to the micro-grid at bus9 through AC/DC converters. Additionally, the grid has two photovoltaic (PV) generation units. Each PV unit has a 1 kV array voltage regulated by a maximum power point tracking algorithm. The PV units are

interfaced through DC/DC converters to the grids with a voltage of 5 kV. Three DC loads are connected to the grid, as well. The rated powers of these loads, as mentioned, are 1 MW, 3 MW, and 4 MW with rated voltage of 1.5 kV at buss 3, 7, and 11, respectively. DC/DC converters are used to reduce the voltage and interface those loads.

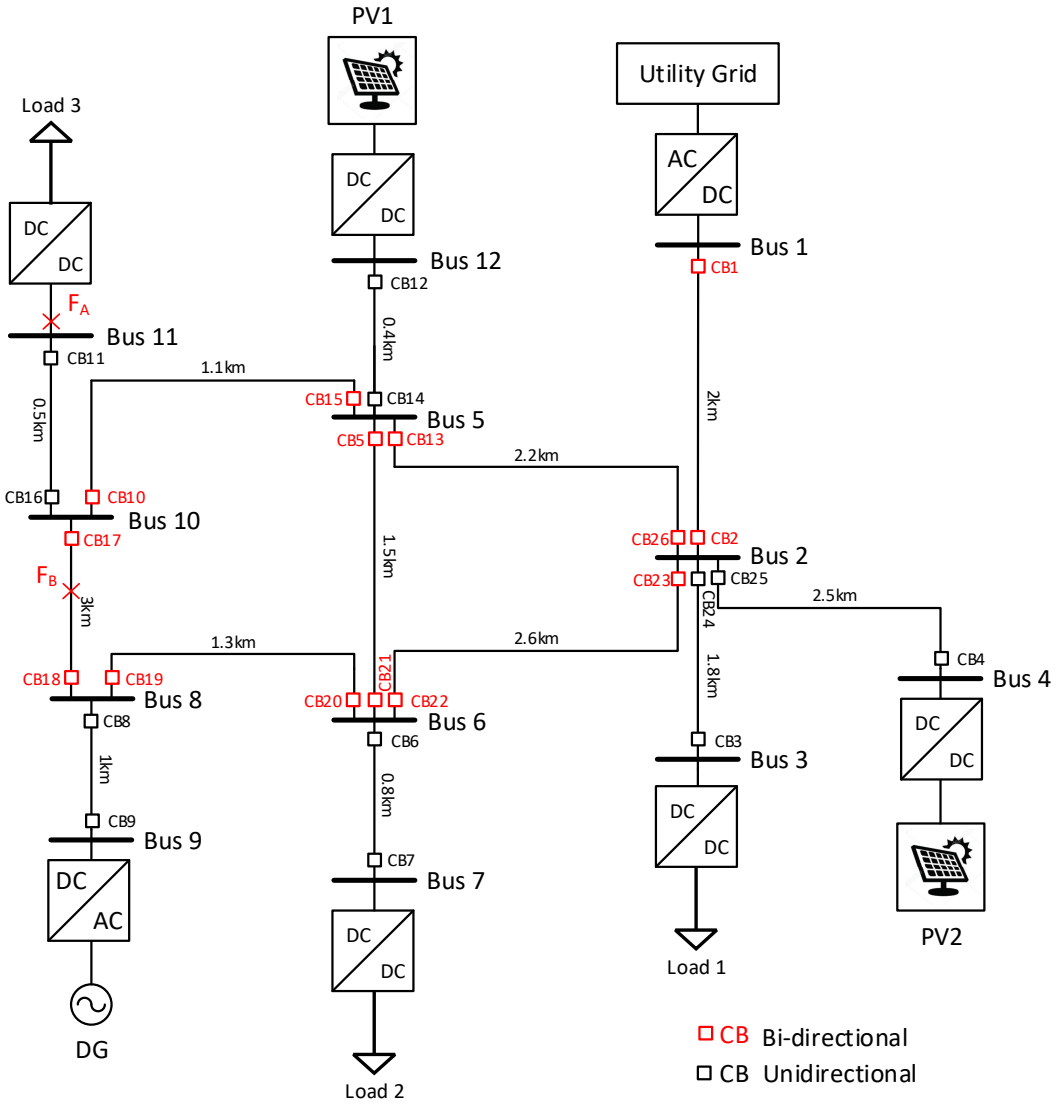

Figure 12. Medium-voltage DC (MVDC) 12-bus micro-grid study case.

According to the structure of the proposed grid, three types of DC faults can occur. These faults are pole-pole (P-P), positive pole-ground (P-G), and negative pole-ground (N-G) [32,35,36]. Additionally, in some of the grid lines, the power flow has a probability of being in the opposite direction after the fault clears and disconnects the faulty zone. These lines should be equipped with bi-directional circuit breakers to allow the power to flow in the other direction.

The protection scheme for the loads, lines, and sources is shown in Figure 12, where bidirectional and unidirectional circuit breakers are placed to protect the grid. Whether unidirectional or bidirectional breaker, the need to place circuit breakers on the power line depends on the power flow in that line. In that aspect, the bidirectional coupled inductors breakers are placed on the lines that have expected power flow in both directions. Meanwhile, the unidirectional breakers are placed to detect the faults in the zones of sources and loads, so there is one expected power flow. The description of the breakers is shown in Table 4.

Table 4. Description of the protection scheme circuit breakers.

Circuit Breaker Numbers	Type
CB3, CB4, CB6, CB7, CB8, CB9, CB11, CB12, CB14, CB16, CB24, and CB25	Unidirectional
CB1, CB2, CB5, CB10, CB13, CB15, CB17, CB18, CB19, CB20, CB21, CB22, CB23, and CB26	Bi-directional

The bi-directional proposed circuit breaker (Y-source network) does not need to detect the fault location to interrupt the overcurrent. Therefore, the CB response is completely automatic, and the gate signals do not control the operation of the breaker during the fault conditions. In particular cases, an external control to SCRs gate signals is required, such as maintenance, power flow direction changes before reaching the steady-state (during transient) where the current is high, and after the fault is clear. There are three options to control the operation of the grid breakers, which are central, local, and paired breaker controls [22].

In the central control, all breakers are controlled by a main unit. This unit receives information from each circuit breaker. This information contains the input and the output current compared with a threshold value. Depending on this information, if the output current is larger than a large threshold value, it means the breaker experienced a fault, and a minimum number of breakers should be off to isolate the fault. Additionally, the input current of the breaker is compared to a small value of threshold to know if the breaker switched ON or OFF. In addition, the central control unit is able to send gate signals through a communication system to the SCRs of the breakers to make them operate as DC switches [22].

The second option of the breaker control is local breaker control. In this option, the output current to the input current for each circuit breaker is monitored. If these currents are similar means, the breaker works under normal conditions. In another case, if these currents are different, the breaker should be an open state [22]. In the case of bi-directional breakers, clearing a faulty zone causes a reverse current in the different breaker. During that, the current goes to zero. The circuit breaker has no gate signal to allow the breaker to pass the current in the opposite direction. The local control of the breakers responds to indicate the change in the power flow and gates the SCRs with signals that give the required direction of the power flow. An example for this case, in the MVDC system that is shown in Figure 12, if a fault occurs at bus11 and the breaker at that bus will isolate the faulty bus, the current between bus 5 and bus 10 will be in the opposite direction. In this case, the circuit breakers CB10 and CB15 should be gated to switch them back ON and allow the current to pass through the line in the other direction.

The third option, utilized in this work, of the breaker control, is paired or matching breaker control. This option of control can be applied for breakers that operate in the same path of current. These breakers can receive gate signals at the same time and operate together as a pair. The paired breakers pass the same current or cut that current off. In that aspect, both paired breakers turn off regardless of which breaker takes action to clear the fault [22]. For example, in the system of Figure 12, breakers CB17 and CB18 are shared to conduct the current of the line between buses 8 and 10. Their SCRs gate signals should be applied at the same time to conduct them and allow the current to flow through the line. Table 5 shows the breaker pairs and their locations.

Table 5. Paired circuit breakers and their locations.

Paired Breakers	Location	Paired Breakers	Location
CB11, CB16	Bus 10–Bus 11	CB17, CB18	Bus 10–Bus 8
CB14, CB12	Bus 5–Bus 12	CB19, CB20	Bus 6–Bus 8
CB1, CB2	Bus 1–Bus 2	CB5, CB21	Bus 5–Bus 6
CB4, CB25	Bus 2–Bus 4	CB22, CB23	Bus 2–Bus 6

Table 5. *Cont.*

Paired Breakers	Location	Paired Breakers	Location
CB3, CB24	Bus 2–Bus 3	CB10, CB15	Bus 5–Bus 10
CB6, CB7	Bus 6–Bus 7	CB26, CB13	Bus 2–Bus 5
CB8, CB9	Bus 8–Bus 9		

The test grid of Figure 12 is simulated by using MATLAB software. The grid has two levels of voltage ±2.5 kV with different lengths of lines, as shown in the grid diagram. The DC/DC boost converter is designed to build step-up converters that are located in buses 4 and 12. These converters are used to connect the photovoltaics (PVs) to the grid. The distribution generator and the AC grid are connected to the grid through VSCs. DC loads are connected to the grid through DC/DC buck converters to reduce the voltage and drive the loads that are connected to buses 3, 7, and 11. According to the expected power flow, the circuit breakers are required to be bidirectional in some zones as explained in the protection scheme of Figure 12.

In the first event, a pole-to-pole fault will apply at bus 11, where the fault position is represented by point F_A as shown in Figure 12. Bus 11 feeds a load of 4MW load through a DC/DC converter. The breaker CB11 will cut off the bus current and disconnect the converter and the load. Figure 13a shows that the current of bus 11 reaches zero when the fault occurs by the action of the unidirectional breaker, which is CB11. The load of the 4 MW is disconnected, and the current in the line between bus 10 and bus 11 is zero. The current of the line that is connected between bus 5 and bus 10 is changed and reduced from 700.85A to 63A, as shown in Figure 13c.

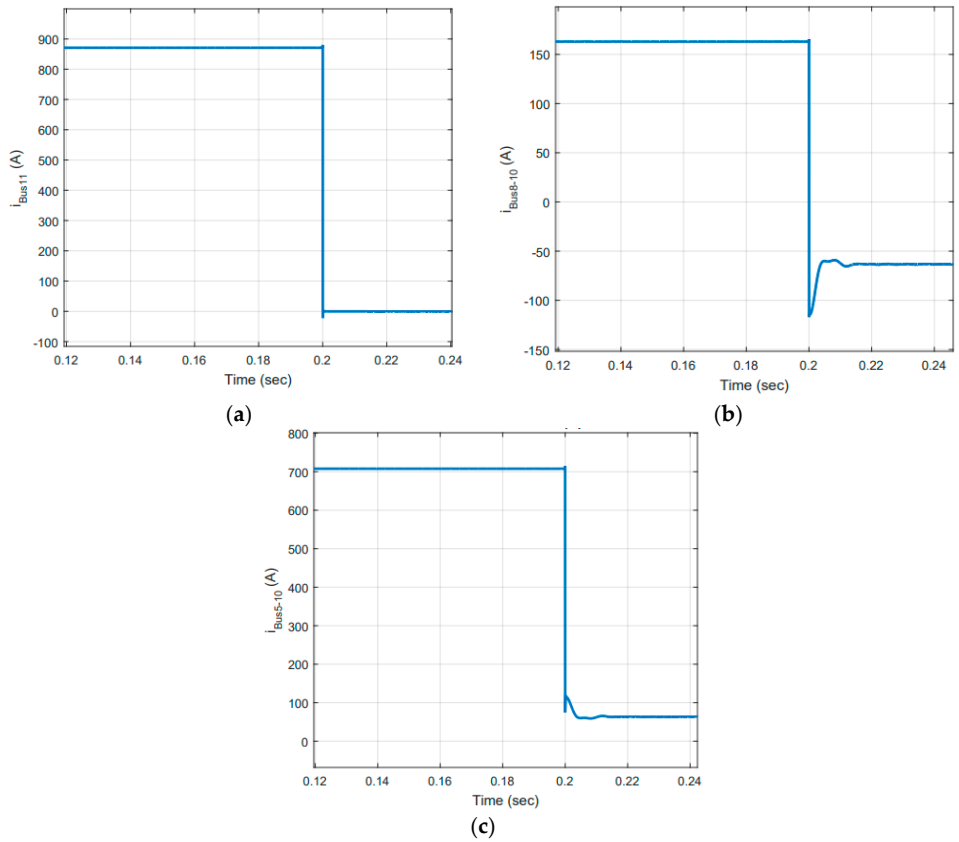

Figure 13. Currents during the fault occurring at bus 11, (**a**) current waveform of bus 11, (**b**) current waveform of bus 8 to bus 10, and (**c**) current waveform of bus 5 to bus 10.

The same current of the line between bus 5 and bus 10 will pass through the line of bus 10–8. The direction of that current will be opposite its direction before the occurrence of the fault and disconnect 4MW load; Figure 13c shows that current. At that point, the circuit breakers CB17 and CB18 placed on the line between bus 8 and bus 10 should be bi-directional breakers to allow the power to flow from bus 10 to bus 8. Figure 13b shows the line current between bus 8 and bus 10 is changed from its original positive value to the negative. Based on that, the Y-source breakers placed on this line allow the current flow in the opposite direction.

In order to test the bi-directional Y-source breaker, a fault will apply at the middle of the line between bus 8 and 10 as represented by point F_B as shown in Figure 12. The fault will apply after the current of the line flows in the opposite direction. CBs 17 and 18 will respond and take action to reduce the line current to zero immediately when the fault occurs. Figure 14a,b illustrate the current waveforms of the lines between bus 8–10 and bus 5–10, respectively. The current of CBs 10 and 15 goes to zero also after clearing the faults because the CB11 is still open and load 3 is disconnected, so the power through the line between bus 5 and 10 flows only through the line between bus 10–8.

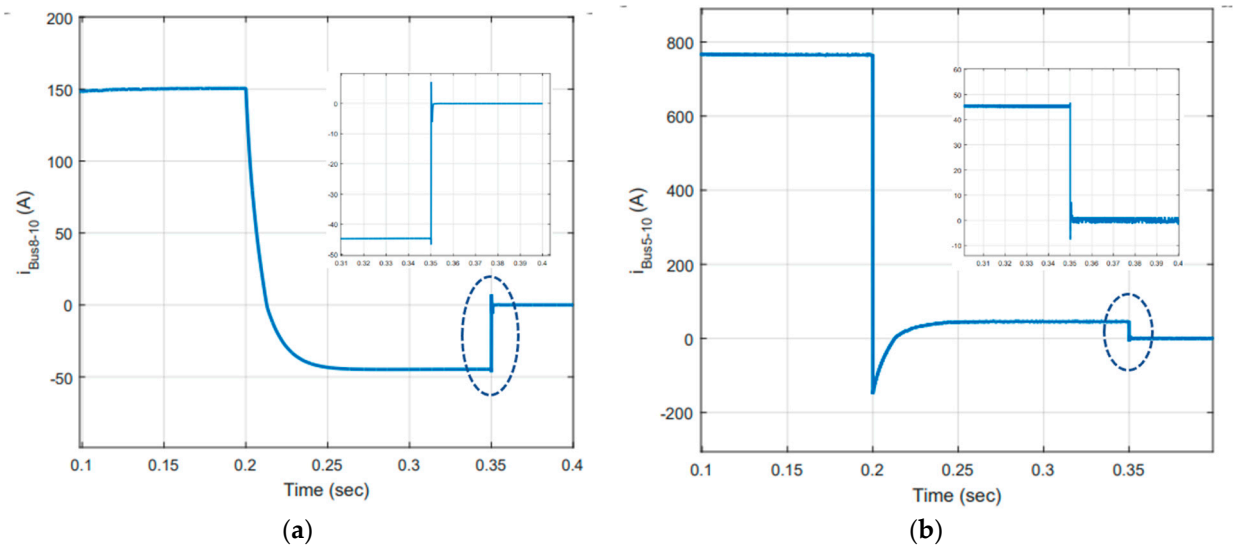

Figure 14. Current waveforms during fault occurring in the middle of the line between bus 8 and bus 10: (**a**) Bus 8-bus 10 and (**b**) Bus 5-bus 10.

4. Conclusions

The Y-source impedance network is used to build a bi-directional solid-state circuit breaker for MVDC systems. The breaker frequency response demonstrates that the reflected current to the source through the SCRs is higher than their forward current. This current forces the SCRs to commutate OFF during the fault conditions. The coupling levels among the inductors of the breaker affect the value of the reflected current. The proposed breaker has the ability to interrupt the fault current if the magnetic coupling level is higher than a specific level, which is called a null condition. The turns−ratio affects this value, where an increase in the turns-ratio causes decreasing in the required level of the coupling. The fault conductance must have a minimum value and slope rate in order to make the Y-source breaker products an adequate reflected current to drop the forward SCRs current to zero. The simulation results verify the operation of the breaker with a fault condition, where the minimum value of the source current is affected by the level of the coupling. The condition of a load change is simulated, and the results verify that the breaker allows the load current to change without interrupting the source current. The Y-source breaker is developed to clear the fault current during the different expected types of fault in the MVDC systems. The simulation results approved the ability of the developed breaker to reduce the positive

and negative pole currents to zero during three types of occurring faults. The proposed protection scheme for a 12-bus, ±2.5 kV micro-grid is tested by applying a fault at two different locations in the grid. The Y-source proposed breaker is connected to the lines that may conduct the power in both directions. During the first fault event, the breaker located nearby the fault point interrupts the current and isolates the faulty zone. That causes passing an opposite current in an adjacent line. Based on the obtained results, the Y-source breaker allowed this current to pass in the opposite direction. The second fault event is applied at the line where the Y-source breakers are placed. In this case, the results show that the Y-source breaker clears the fault by reducing the current naturally to zero. The results verify the ability of the breaker to allow the normal current to pass and to interrupt the abnormal current in both directions.

Author Contributions: Conceptualization, H.A.-k.; methodology, H.A.-k.; software, H.A.-k.; validation, H.A.-k.; formal analysis, H.A.-k.; investigation, H.A.-k.; resources, H.A.-k.; writing–original draft preparation H.A.-k.; writing—review and editing, J.A.; visualization, J.A.; supervision, J.A.; project administration, J.A. Both authors have read and agreed to the published version of the manuscript.

Funding: This research received no external funding. The APC is funded by the authors.

Institutional Review Board Statement: Not applicable.

Informed Consent Statement: Not applicable.

Data Availability Statement: The data presented is contained in the article.

Conflicts of Interest: The authors declare no conflict of interest.

References

1. Wang, R.; Zhang, B.; Zhao, S.; Liang, L.; Chen, Y. Design of an IGBT-series-based solid-state circuit breaker for battery energy storage system terminal in solid-state transformer. In Proceedings of the IECON 2019—45th Annual Conference of the IEEE Industrial Electronics Society, Lisbon, Portugal, 14–17 October 2019; Volume 1, pp. 6677–6682.
2. Cui, S.; Hu, J.; De Doncker, R.W. Fault-Tolerant Operation of a TLC-MMC Hybrid DC-DC Converter for Interconnection of MVDC and HVdc Grids. *IEEE Trans. Power Electron.* **2020**, *35*, 83–93. [CrossRef]
3. Shi, Y.; Li, H. Isolated Modular Multilevel DC–DC Converter with DC Fault Current Control Capability Based on Cur-rent-Fed Dual Active Bridge for MVDC Application. *IEEE Trans. Power Electron.* **2018**, *33*, 2145–2161. [CrossRef]
4. IEEE Std 1709–1018. *IEEE Recommended Practice for 1 kV to 35 kV Medium-Voltage DC Power Systems on Ships*; IEEE: New York, NY, USA, 2018; pp. 1–54.
5. Kumar, D.; Zare, F.; Ghosh, A. DC Microgrid Technology: System Architectures, AC Grid Interfaces, Grounding Schemes, Power Quality, Communication Networks, Applications, and Standardizations Aspects. *IEEE Access* **2017**, *5*, 12230–12256. [CrossRef]
6. Keshavarzi, D.; Ghanbari, T.; Farjah, E. A Z-Source-Based Bidirectional DC Circuit Breaker with Fault Current Limitation and Interruption Capabilities. *IEEE Trans. Power Electron.* **2016**, *32*, 6813–6822. [CrossRef]
7. Corzine, K.A. Circuit breaker for DC micro grids. In Proceedings of the 2015 IEEE First International Conference on DC Microgrids (ICDCM), Atlanta, GA, USA, 7–10 June 2015.
8. Li, C.; Nie, Z.; Li, H.; Zhang, Y. A novel solid-state protection scheme for DC system. In Proceedings of the 2016 IEEE 8th International Power Electronics and Motion Control Conference (IPEMC-ECCE Asia), Hefei, China, 22–26 May 2016; pp. 2039–2042.
9. Maqsood, A.; Corzine, K. Z-source Dc circuit breakers with coupled inductors. In Proceedings of the 2015 IEEE Energy Conversion Congress and Exposition (ECCE), Montreal, QC, Canada, 20–24 September 2015; pp. 1905–1909.
10. Lin, W.; Jovcic, D.; Nguefeu, S. Saad, H. Modelling of high-power hybrid DC circuit breaker for grid-level studies. *IET Power Electron.* **2016**, *9*, 237–246. [CrossRef]
11. Salomonsson, D.; Soder, L.; Sannino, A. Protection of Low-Voltage DC Microgrids. *IEEE Trans. Power Deliv.* **2009**, *24*, 1045–1053. [CrossRef]
12. Cuzner, R.M.; Venkataramanan, G. The status of DC micro-grid protection. In Proceedings of the 2008 IEEE Industry Applications Society Annual Meeting, Edmonton, AB, Canada, 5–9 October 2008; pp. 1–8.
13. Baran, M.E.; Mahajan, N.R. Overcurrent Protection on Voltage-Source-Converter-Based Multiterminal DC Distribution Systems. *IEEE Trans. Power Deliv.* **2007**, *22*, 406–412. [CrossRef]
14. Tennakoon, S.; McEwan, P. Short-circuit interruption performance of thyristor circuit breakers. In Proceedings of the 1994 IEEE Applied Power Electronics Conference and Exposition—ASPEC'94, Orlando, FL, USA, 13–17 February 1994.
15. Corzine, K. Dc micro grid protection with the z-source breaker. In Proceedings of the 39th Annual Conference of the IEEE Industrial Electronics Society, Vienna, Austria, 10–13 November 2013.

16. Bolanowski, B.; Wojcik, F. A fast DC hybrid circuit breaker. In Proceedings of the IEE Colloquium on Electronic-Aided Current-Limiting Circuit Breaker Developments and Applications, London, UK, 22 November 1989.
17. Meyer, C.; Kowal, M.; De Doncker, R. Circuit breaker concepts for future high-power DC-applications. In Proceedings of the Fourtieth IAS Annual Meeting. Conference Record of the 2005 Industry Applications Conference, Hong Kong, China, 2–6 October 2005; Volume 2, pp. 860–866.
18. Hirayama, S.Y. Zero-Current Arc-Suppression DC Circuit Breaker. U.S. Patent 4,740,858, 26 April 1988.
19. Niwa, Y.; Matsuzaki, J.; Yokokura, K. The basic investigation of the high-speed VCB and its application for the DC power system. In Proceedings of the 23rd International Symposium on Discharges and Electrical Insulation in Vacuum, Bucharest, Romania, 15–19 September 2008; Volume 1, pp. 107–112. [CrossRef]
20. Lawes, D.; Ran, L.; Xu, Z. Design of a solid-state D.C. circuit breaker for light rail transit power supply network. In Proceedings of the 2014 IEEE Energy Conversion Congress and Exposition (ECCE), Pittsburgh, PA, USA, 14–18 September 2014; pp. 350–357.
21. Shen, Z.J.; Sabui, G.; Miao, Z.; Shuai, Z. Wide-Bandgap Solid-State Circuit Breakers for DC Power Systems: Device and Circuit Considerations. *IEEE Trans. Electron Devices* **2015**, *62*, 294–300. [CrossRef]
22. Maqsood, A.; Corzine, K. DC Microgrid Protection: Using the Coupled-Inductor Solid-State Circuit Breaker. *IEEE Electrif. Mag.* **2016**, *4*, 58–64. [CrossRef]
23. Corzine, K.A.; Ashton, R.W. A New Z-Source DC Circuit Breaker. *IEEE Trans. Power Electron.* **2012**, *27*, 2796–2804. [CrossRef]
24. Corzine, K.A.; Ashton, R.W. Structure and analysis of the Z-source MVDC breaker. In Proceedings of the 2011 IEEE Electric Ship Technologies Symposium, Alexandria, VA, USA, 10–13 April 2011; pp. 334–338.
25. Chang, A.H.; Avestruz, A.-T.; Leeb, S.B.; Kirtley, J.L. Design of DC system protection. In Proceedings of the 2013 IEEE Electric Ship Technologies Symposium (ESTS), Arlington, VA, USA, 22–24 April 2013; pp. 500–508.
26. Chang, A.H.; Sennett, B.R.; Avestruz, A.-T.; Leeb, S.B.; Kirtley, J.L. Analysis and Design of DC System Protection Using Z-Source Circuit Breaker. *IEEE Trans. Power Electron.* **2016**, *31*, 1036–1049. [CrossRef]
27. Maqsood, A.; Overstreet, A.; Corzine, K.A. Modified Z-source DC Circuit Breaker Topologies. *IEEE Trans. Power Electron.* **2016**, *31*, 7394–7403. [CrossRef]
28. Al-Khafaf, H.; Asumadu, J. Γ-Z-source DC circuit breaker operation with variable coupling coefficient k. In Proceedings of the 2017 IEEE International Conference on Electro Information Technology (EIT), Lincoln, NE, USA, 14–17 May 2017; pp. 492–496.
29. Al-Khafaf, H.; Asumadu, J. Bi-directional Y-Source DC Circuit Breaker Design and Analysis Under Different Conditions of Coupling. In Proceedings of the 2018 9th IEEE International Symposium on Power Electronics for Distributed Generation Systems (PEDG), Charlotte, NC, USA, 25–28 June 2018; pp. 1–6.
30. Al-Khafaf, H.; Asumadu, J. Y-Source Bi-directional DC Circuit Breaker. In Proceedings of the 2018 International Power Electronics Conference (IPEC-Niigata 2018 -ECCE Asia), Niigata, Japan, 20–24 May 2018.
31. Witulski, A. Introduction to modeling of transformers and coupled inductors. *IEEE Trans. Power Electron.* **1995**, *10*, 349–357. [CrossRef]
32. Saleh, K.A.; Hooshyar, A.; El-Saadany, E.F. Ultra-High-Speed Traveling-Wave-Based Protection Scheme for Medi-um-Voltage DC Microgrids. *IEEE Trans. Smart Grid* **2019**, *10*, 1440–1451. [CrossRef]
33. Monad, M.; Gavriluta, C.; Luna, A.; Candela, J.I.; Rodriguez, P. Centralized Protection Strategy for Medium Voltage DC Microgrids. *IEEE Trans. Power Deliv.* **2017**, *32*, 430–440. [CrossRef]
34. Li, W.; Monti, A.; Ponci, F. Fault detection and classification in medium fault detection and classification in medium wavelets and artificial neural networks. *IEEE Trans. Instrum. Meas.* **2014**, *63*, 2651–2665. [CrossRef]
35. Li, H.; Li, W.; Luo, M.; Monti, A. Design of Smart MVDC Power Grid Protection. *IEEE Trans. Instrum. Meas.* **2011**, *60*, 3035–3046. [CrossRef]
36. Tang, L.; Ooi, B.-T. Locating and Isolating DC Faults in Multi-Terminal DC Systems. *IEEE Trans. Power Deliv.* **2007**, *22*, 1877–1884. [CrossRef]